

# Cavity-Enabled Enhancement of Ultrafast Intramolecular Vibrational Redistribution over Pseudorotation

**Authors:** Teng-Teng Chen<sup>1†</sup>, Matthew Du<sup>1†</sup>, Zimo Yang<sup>2</sup>, Joel Yuen-Zhou<sup>1\*</sup>, Wei Xiong<sup>1,2,3\*</sup>

## Affiliations:

<sup>1</sup>University of California, San Diego, Department of Chemistry and Biochemistry, La Jolla, CA

<sup>2</sup>University of California, San Diego, Materials Science and Engineering Program, La Jolla, CA

<sup>3</sup>University of California, San Diego, Department of Electrical and Computer Engineering, La Jolla, CA

\* Corresponding author. Email: [joelyuen@ucsd.edu](mailto:joelyuen@ucsd.edu) (Joel Yuen-Zhou) and [w2xiong@ucsd.edu](mailto:w2xiong@ucsd.edu) (Wei Xiong)

†These authors contributed equally to this work.

**Abstract:** We studied a single-step ultrafast energy exchange process of  $\text{Fe}(\text{CO})_5$  under vibrational strong coupling (VSC), with the aim of elucidating the influence of VSC on chemical reactions.  $\text{Fe}(\text{CO})_5$  has two competing channels to exchange energy between vibrational modes: pseudorotation and intramolecular vibrational energy redistribution (IVR). Ultrafast infrared spectroscopy shows that under VSC, when polaritons are excited, the overall vibrational energy exchange dynamics are accelerated, with IVR becoming faster than pseudorotation. In contrast, the vibrational dynamics initiated in the dark modes under VSC remain unchanged. This work demonstrates that initialization through polariton and reservoir states can afford different dynamics and suggests that the basic concept of VSC-modified chemistry – polaritons can influence reactions – holds, regardless of current controversies over the thermally-activated VSC-modified reactions.

Vibrational strong coupling (VSC) gives rise to delocalized superpositions of molecular vibrations and electromagnetic modes (cavity modes), known as molecular vibrational polaritons(1-3). Recently, VSC has arisen as a promising handle to manipulate chemical reactions in condensed phases(4-9). Extensive experimental evidence has shown that, without photoexcitation, reaction rates can be either accelerated or decelerated by VSC, and reaction selectivity can even be altered(4-6, 8). While much effort has been devoted to providing a sound explanation for VSC-modified chemistry, consensus between theory and experiments is still missing(10-17). Though it is clear that polaritons are different from bare molecular states, and thereby have the potential to modify chemistry, dark modes, which greatly outnumber polaritons, have the same excitation energies as the uncoupled vibrational modes(18). Hence, some theoretical work predicts that reactivity in the collective VSC regime is similar to that outside an optical cavity(11, 13-15, 19, 20), which is consistent with a couple of recent experimental results showing no modification of reactions from VSC(16, 21). Resolution of the discrepancies is hindered by the following factors: most reactions studied so far are quite complex, *i.e.*, involve multiple steps or are diffusion limited, and reactions involving both dark modes and polaritons are probed together(4-8). To delineate the effect of VSC, it is therefore critical to study elementary reactions and use a technique that can differentiate the contributions from polaritons and dark modes.

In this work, we used ultrafast two-dimensional infrared (2D IR) spectroscopy to follow how the polaritons and dark modes evolve in both pseudorotation and intramolecular energy redistribution (IVR) of  $\text{Fe}(\text{CO})_5$ (22). We did so in a state-resolved manner, thereby meeting the desired criteria listed above.  $\text{Fe}(\text{CO})_5$  features two infrared (IR) active vibrational bands, a doubly degenerate  $e'$  mode at  $1999\text{ cm}^{-1}$  involving three equatorial CO groups and an  $a_2''$  mode at  $2022\text{ cm}^{-1}$  involving the axial CO groups (Fig. S1). Harris and co-workers applied 2D IR spectroscopy and showed that  $\text{Fe}(\text{CO})_5$  can rearrange from its  $D_{3h}$  equilibrium geometry to a  $C_{4v}$  transition state and back to  $D_{3h}$ , during which the equatorial and axial CO ligands interconvert, leading to vibrational energy exchange between  $a_2''$  and  $e'$  modes (23). This process, referred to as Berry's pseudorotation, is a single barrier crossing and thus represents the essence of elementary reactions, although the product is indistinguishable from the reactant(24). Given that Berry's pseudorotation competes with IVR between  $a_2''$  and  $e'$  modes whose transition dipoles are perpendicular to each other (Fig. 1A top),  $\text{Fe}(\text{CO})_5$  is an ideal testbed to understand how VSC affects single barrier crossing events and the branching ratio between various dynamical processes.

Using 2D IR spectroscopy, we found that, when polaritons are pumped, they can accelerate the overall 2D IR cross peak dynamics and, more interestingly, makes IVR faster than pseudorotation (Fig.1A bottom). In contrast, the dynamics triggered by exciting the dark reservoir modes are similar to the dynamics of molecules outside the cavity. Thus, the fundamental concept of VSC-modified chemistry – polaritons can change reactions – holds. However, because dark modes are statistically dominant, the overall influence of VSC on the dynamics of the  $\text{Fe}(\text{CO})_5$ , when measured without differentiating polariton and dark modes (*e.g.*, without optical pumping at room temperature), should be negligible.

The VSC condition was achieved by placing a solution of  $\text{Fe}(\text{CO})_5$  in *n*-dodecane into a Fabry-Pérot microcavity. Unless specifically mentioned, we set the  $\text{Fe}(\text{CO})_5$  concentration to  $\sim 180\text{ mM}$  and the cavity longitudinal thickness to  $\sim 12.5\text{ }\mu\text{m}$ . The  $e'$  and  $a_2''$  vibrational modes of  $\text{Fe}(\text{CO})_5$  strongly couple to a 5<sup>th</sup>-order cavity mode. The IR spectrum (Fig. 1B) shows the transitions of upper, middle, and lower polaritons (UP, MP and LP) at  $\omega_{\text{UP}} = 2045$ ,  $\omega_{\text{MP}} = 2014$ , and  $\omega_{\text{LP}} = 1976\text{ cm}^{-1}$ , respectively. By fitting to a coupled oscillator model (see SI Section 2.1),

we determined that the cavity mode is  $2013\text{ cm}^{-1}$  and interacts with the  $e'$  and  $a_2''$  modes with amplitudes  $g_{\text{cav}-e'} = 26\text{ cm}^{-1}$  and  $g_{\text{cav}-a_2''} = 19\text{ cm}^{-1}$ , respectively. Because the full width at half maximum (FWHM) of the  $e'$  and  $a_2''$  modes are  $8\text{ cm}^{-1}$  and  $5\text{ cm}^{-1}$ , respectively, and that of the cavity mode is  $11\text{ cm}^{-1}$ , the samples satisfy the criteria for VSC(25).

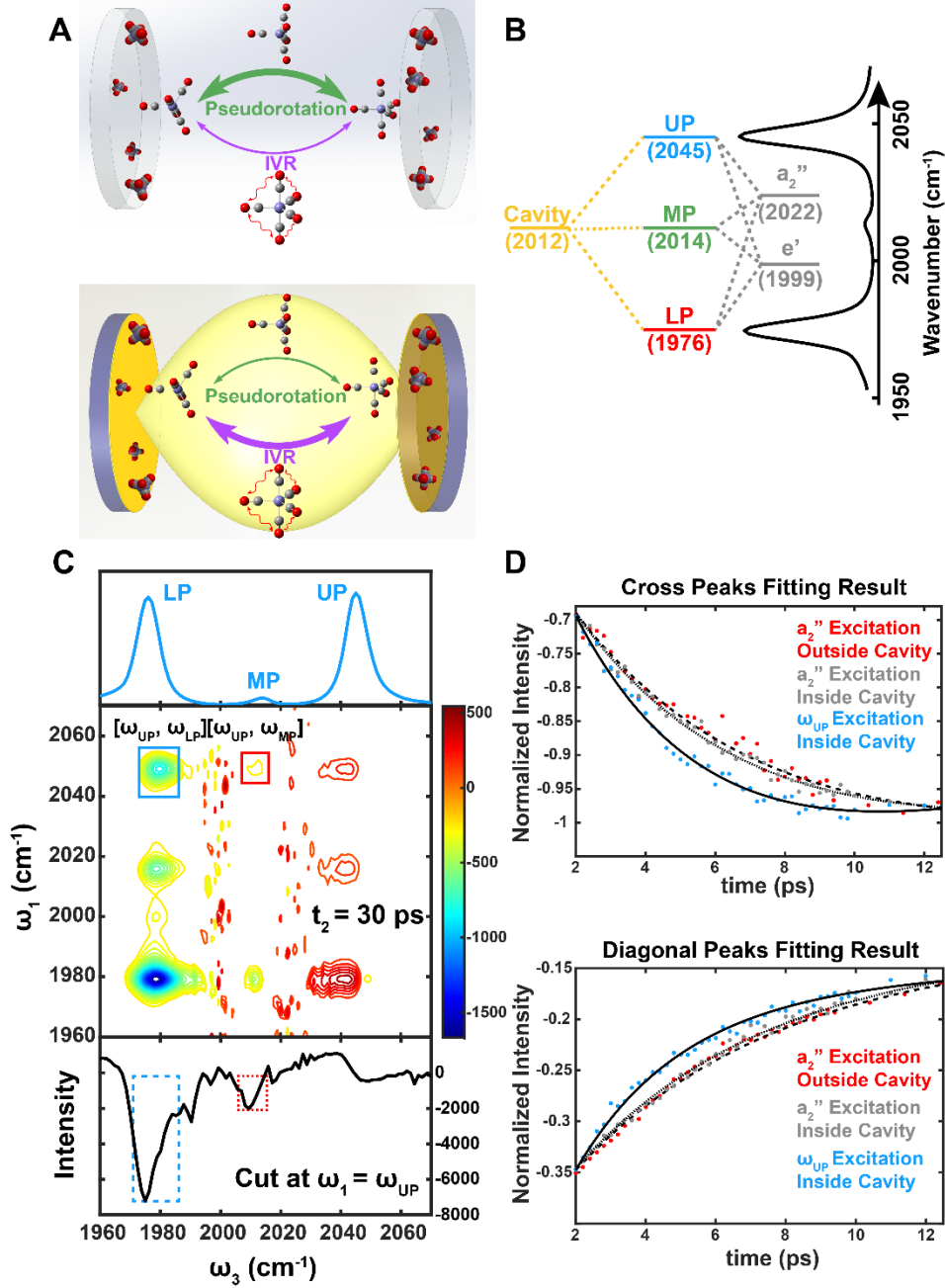


Fig. 1 Influence of VSC on  $\text{Fe}(\text{CO})_5$  energy exchange dynamics. (A) Schematic drawing showing that, when  $\text{Fe}(\text{CO})_5$  is outside of cavity, pseudorotation is the dominating channel (top); when the molecule is placed in an optical cavity, IVR becomes the dominant energy exchange process while pseudorotation is suppressed (bottom). (B) Strong coupling diagram and IR spectrum of  $\text{Fe}(\text{CO})_5$  inside the cavity. (C) Normalized 2D IR spectrum using linear spectrum of strongly coupled  $\text{Fe}(\text{CO})_5$  at  $t_2 = 30\text{ ps}$  in dodecane (blue and red boxes represent  $[\omega_{\text{UP}}, \omega_{\text{LP}}]$  and  $[\omega_{\text{UP}}, \omega_{\text{MP}}]$  peaks, respectively), along with the corresponding linear spectrum (top panel) and normalized narrowband pump probe spectrum at  $\omega_1 = \omega_{\text{UP}}$  (bottom panel). (D) Experimental dynamics of cross peaks (top panel) and diagonal peaks

(bottom panel) for  $\text{Fe}(\text{CO})_5$  outside the cavity upon pumping of the  $a_2''$  modes (red dots) and inside the cavity upon pumping of UP (blue dots) and the  $a_2''$  dark modes (gray dots). The black dashed, dotted and solid lines are the corresponding fits. Energy is exchanged at a faster rate when pumping UP, whereas pumping the  $a_2''$  dark modes leads to a similar rate to the one outside the cavity.

We used 2D IR to monitor the cross-peak dynamics both outside and inside the cavity (26-29). Through pseudorotation and IVR, the  $a_2''$  and  $e'$  modes can exchange energy. By measuring the dynamics of the [2022, 1986] cross and [2022, 2010] diagonal peaks of the 1- $\rightarrow$ 2 transitions (Fig. S6) and fitting them to a kinetic model (see SI Section 2.3.1), we determined the energy exchange rate constant  $k_{ex}$  to be  $(0.084 \pm 0.002) \text{ ps}^{-1}$  at 25 °C (Fig. 1D). Here, unless specifically mentioned, all measurements are done under magic angle conditions to remove contributions from rotational dynamics.

Similarly, for  $\text{Fe}(\text{CO})_5$  under VSC (Fig. 1C, bottom), we followed the dynamics of the  $[\omega_{UP}, \omega_{MP}]$  (red box in Fig. 1C) and  $[\omega_{UP}, \omega_{LP}]$  (blue box in Fig. 1C) peaks of the 2D IR spectrum (or the corresponding narrowband pump probe spectra; see SI Section 1.3 for details). Here we specifically focus on the dynamics involving pumping UP, to avoid complications of hot (*i.e.*, highly excited) vibrational states when exciting LP modes (30). The interpretation of these peaks was discussed in our previous works (27). Basically, the polariton transitions at  $\omega_{MP}$  and  $\omega_{LP}$  overlap with the 1- $\rightarrow$ 2 transition of the  $a_2''$  and  $e'$  modes, respectively (this assignment is further confirmed by spectral simulations (SI Section 2.6) and input-output theory (SI Section 4)). Upon exciting UP, when the waiting time is beyond the polariton lifetime, the  $[\omega_{UP}, \omega_{MP}]$  and  $[\omega_{UP}, \omega_{LP}]$  peaks correspond respectively to the excited state population of the  $a_2''$  and  $e'$  modes. Therefore, the dynamics of these peaks report the energy transfer between the  $a_2''$  and  $e'$  modes facilitated by pseudorotation and IVR. At a first glance, the dynamics under VSC are a bit faster than the one without (Fig.1D).

To quantify the energy exchange dynamics upon pumping UP, we used the kinetic model shown in Fig.2A. First, the population of UP relaxes to both the  $a_2''$  and  $e'$  dark modes within the polariton lifetime. Then, the  $a_2''$  and  $e'$  dark modes exchange energy, through pseudorotation and IVR, and at the same time dissipate energy to their environment. The solution of this kinetic model provides a good fit to the  $[\omega_{UP}, \omega_{MP}]$  and  $[\omega_{UP}, \omega_{LP}]$  dynamics (Fig.2B). Furthermore, the measured dynamics can be separated into three components: polariton relaxation to dark modes at short times (cavity leakage is implicitly accounted for; see SI Section 2.3.2), energy exchange at intermediate times, and vibrational decay at long times. From the fitted results,  $k_{ex}$  under VSC is  $0.113 \pm 0.009 \text{ ps}^{-1}$  at room temperature, 30% faster than that outside the cavity.

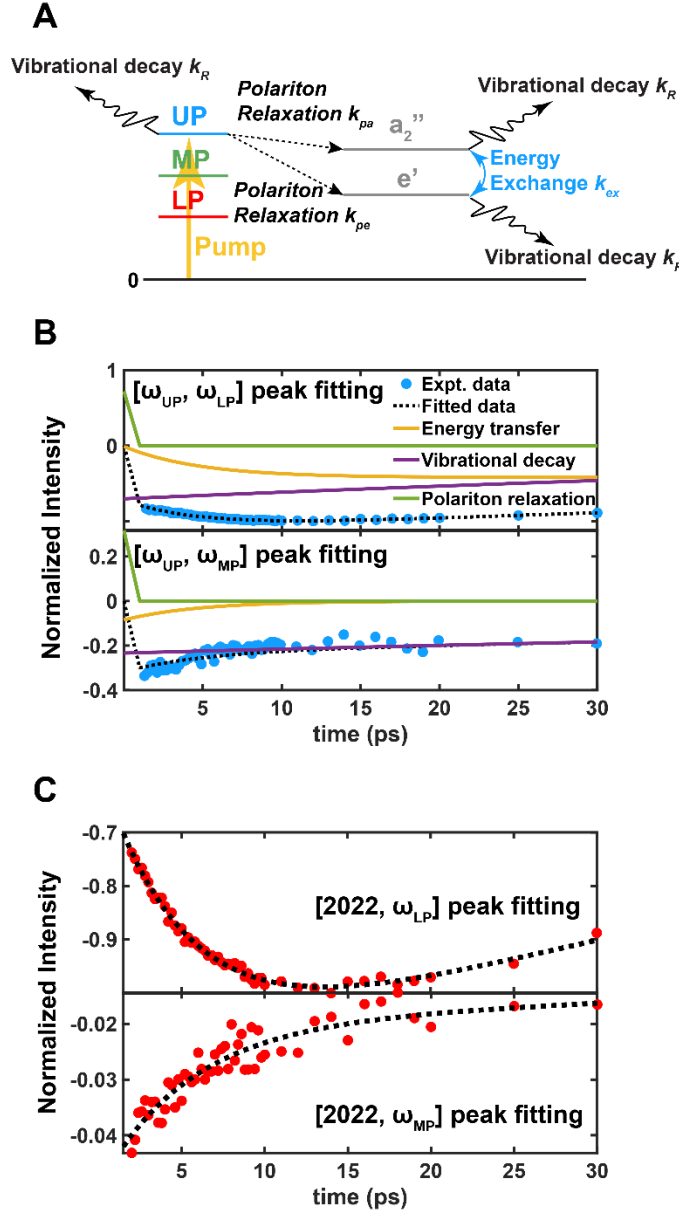


Fig 2 Energy exchange dynamics between  $a_2''$  and  $e'$  modes. (A) Schematic drawing of the kinetic model for  $\text{Fe}(\text{CO})_5$  under VSC. See SI Section 2.3.2 for details of the kinetic model. (B) Experimental data (blue dots) and fits (black dotted lines) including each component for  $[\omega_{UP}, \omega_{LP}]$  (top panel) and  $[\omega_{UP}, \omega_{MP}]$  (bottom panel) peaks. (C) Experimental data (red dots) and fits (black dotted lines) for the  $[2022, \omega_{LP}]$  (top panel) and  $[2022, \omega_{MP}]$  (bottom panel) peaks when the  $a_2''$  dark modes are pumped.

Using 2D IR and the same analysis, we found when exciting the  $a_2''$  dark reservoir modes directly, the energy exchange dynamics have similar trends to those outside the cavity (Fig.2C), and  $k_{ex}$  is  $0.090 \pm 0.006 \text{ ps}^{-1}$ . Clearly, VSC is only modifying the dynamics when the polaritons are pumped, whereas pumping the  $a_2''$  dark reservoir modes causes the system to evolve similarly to the molecules outside the cavity, agreeing with the reservoir's purely molecular character. Similar findings have been predicted by a recent theoretical work (31). The contrast of dynamics between pumping UP and dark  $a_2''$  modes suggests that the energy exchange rates depend on the initial populated states.

Although we have shown that VSC leads to faster energy exchange between the  $a_2''$  and  $e'$  modes, this acceleration could be due to enhancement of either pseudorotation or IVR. To qualitatively distinguish between the two processes, we can measure the vibrational anisotropy (32) associated with the cross peaks. IVR involves energy transfer between  $e'$  and  $a_2''$  modes perpendicular to each other (Fig.3A), while pseudorotation causes energy exchange between  $e'$  and  $a_2''$  modes parallel to each other (Fig.3B). Thus, the anisotropy should start from -0.2 and 0.4 for the former and latter (32-34), respectively. In general, both processes occur concurrently, and the initial anisotropy lies between these values.

Outside the cavity, the initial value of anisotropy is  $\sim 0.06$  for exciting the  $a_2''$  modes (Fig. 3C), suggesting that pseudorotation dominates over IVR. However, under VSC, the opposite trend is observed: the anisotropy starts at  $\sim -0.08$  for exciting UP (Fig. 3D). This contrast indicates that, under VSC, IVR dominates over pseudorotation. Not surprisingly, when pumping the  $a_2''$  dark modes under VSC, the anisotropy is  $\sim 0.06$  (Fig. S18), like the cavity-free case.

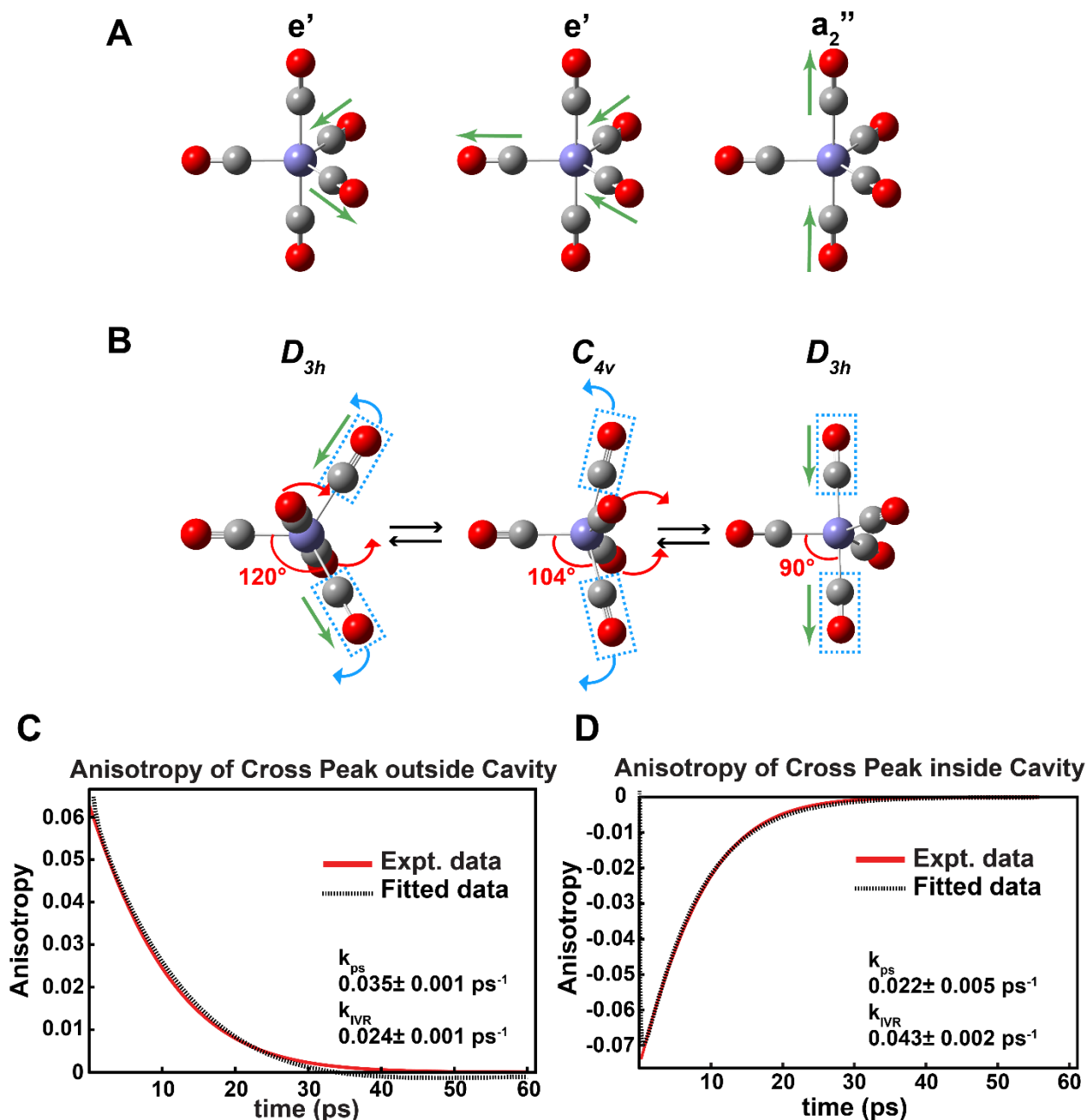


Fig. 3 Cross-peak anisotropy dynamics of IVR and pseudorotation. (A) Depiction of the eigenvectors for the  $a_2''$  and doubly degenerate  $e'$  vibrational modes of  $\text{Fe}(\text{CO})_5$ . IVR leads to energy transfer between modes that are perpendicular to each other. (B) Pseudorotation leads to energy transfer between  $a_2''$  and  $e'$  modes that are parallel to each other. (C, D) Experimental anisotropy (red line) and corresponding fits (black dotted line) for cross peak of  $\text{Fe}(\text{CO})_5$  (C) outside the cavity ([2022, 1986]) and (D) under VSC ([ $\omega_{UP}$ ,  $\omega_{MP}$ ]). Listed are the rate constants, extracted from the fitting, of IVR ( $k_{IVR}$ ) and pseudorotation ( $k_{ps}$ ). The rate constants indicate that VSC accelerates IVR and suppresses pseudorotation.

To determine the rate constants of pseudorotation and IVR, a more detailed kinetic model was developed (see SI Section 2.4)(32-34). The anisotropy can be calculated based on the energy exchange dynamics simulated from the kinetic model. Fitting the measured anisotropy dynamics to the kinetic model, we determined the rate constants for pseudorotation ( $k_{ps}$ ) and IVR ( $k_{IVR}$ ) to be  $0.035 \pm 0.001$  and  $0.024 \pm 0.001$  ps<sup>-1</sup>, respectively, outside the cavity (Fig. 3C) and  $0.022 \pm 0.005$

and  $0.043 \pm 0.002 \text{ ps}^{-1}$  under VSC (Fig. 3D). The former results qualitatively agree with previous work showing that pseudorotation dominates the dynamics outside a cavity(23), except now we quantify the relative contribution of IVR. The quantitative results agree with the qualitative analysis above, indicating that VSC shifts the balance between pseudorotation and other energy exchange channels: outside the cavity, exciting the  $a_2''$  mode yields dynamics where pseudorotation dominates over IVR, while under VSC, exciting the UP promotes IVR and suppresses pseudorotation; yet, under VSC, exciting the  $a_2''$  dark modes does not change the dynamics relative to molecules outside the cavity. We note that this effect is VSC-exclusive, as weak coupling to the cavity does not lead to the modification of the dynamics (SI section 3.4); further, the acceleration of energy transfer and promotion of IVR through VSC is robust against different solvent environments (see results for 1-octanol ,SI Section 3.9).

The sharp contrast between the VSC dynamics starting in UP and  $a_2''$  dark reservoir modes is interesting because, even when UP is excited, the population relaxes to the dark modes on a much shorter time scale than pseudorotation and IVR. The difference then lies in the relaxation processes available to the initial states. Several mechanisms could explain the faster IVR upon pumping UP. For example, the decay from UP to the  $a_2''$  dark modes is accompanied by excitation of low-frequency vibrations (*i.e.*, phonons), and some of these phonons could be further excited during the energetically downhill IVR from  $a_2''$  to  $e'$  modes. It follows that IVR would be accelerated by the first scattering process, and this enhancement would not occur if the system were initialized in the  $a_2''$  dark modes. A limitation of this hypothesis is that, at room temperature, the phonons should have a high occupation number ( $\approx 10$ ), which should not change significantly when UP relaxes to dark modes (through one- or few-phonon excitation). Another possibility is that the VSC-induced speedup in the dynamics reflects a polariton-induced intermolecular vibrational energy transfer. In this case though, the observed anisotropy dynamics should practically be zero, or have a very fast decay(27), instead of starting from a negative value, due to the lack of orientational correlation between donor and acceptor molecules. On the other hand, the mild suppression of pseudorotation is surprising, as it is conventionally thought that these high frequency vibrational modes do not drive the reaction. However, the co-existence of IVR enhancement and pseudorotation suppression suggests otherwise. By quickly going through IVR, molecules may lose their driving force for pseudorotation, leading to its slowdown. It is also possible that the pseudorotation motion is hindered by the phonons excited by the transition from UP to the dark modes. The temperature-dependent measurements further showed that VSC shifts the thermodynamic parameters of activation in the same direction (SI Section 2.4), which has also been observed—and rather consistently—in reports of reaction kinetics altered by VSC(30). This correspondence supports that the insights obtained here should be relevant to understanding the previous experiments(35).

Using 2D IR to resolve ultrafast chemical dynamics with specific initial states, we quantified the energy exchange dynamics in  $\text{Fe}(\text{CO})_5$  under VSC. We showed that when UP is excited under VSC, IVR is promoted and pseudorotation is suppressed compared to the bare molecular system. However, pumping the dark reservoir modes under VSC led to little change in the dynamics compared to outside the cavity. Because the population at thermal equilibrium resides predominantly in the dark modes, the overall influence of VSC on  $\text{Fe}(\text{CO})_5$  should be negligible without external (*e.g.*, laser) pumping. Yet, the present results show an important insight to unify the works reporting VSC-modified reactions and the ones reporting or predicting the opposite – regardless of how reactions behave under thermally-activated conditions, the basic concept of VSC-modified chemistry works: populated polaritons can influence chemical



dynamics. These findings suggest that the future of VSC-modified thermal chemistry lies in controlling the dark modes, with either reducing the number of dark reservoir modes, *e.g.*, through cavity miniaturization, or making dark modes more delocalized through heterogeneity(36-38).

## References and Notes

1. J. P. Long, B. S. Simpkins, *ACS Photonics* **2**, 130-136 (2015).
2. A. Shalabney *et al.*, *Nat. Commun.* **6**, 1-6 (2015).
3. T. W. Ebbesen, *Acc. Chem. Res.* **49**, 2403-2412 (2016).
4. A. Thomas *et al.*, *Angew. Chem. Int. Ed.* **55**, 11462-11466 (2016).
5. A. Thomas *et al.*, *Science* **363**, 615-619 (2019).
6. K. Hirai, R. Takeda, J. A. Hutchison, H. Uji-i, *Angew. Chem. Int. Ed.* **59**, 5332-5335 (2020).
7. Y. Pang *et al.*, *Angew. Chem. Int. Ed.* **59**, 10436-10440 (2020).
8. F. J. Garcia-Vidal, C. Ciuti, T. W. Ebbesen, *Science* **373**, eabd0336 (2021).
9. A. Sau *et al.*, *Angew. Chem. Int. Ed.* **60**, 5712-5717 (2021).
10. J. A. Campos-Gonzalez-Angulo, R. F. Ribeiro, J. Yuen-Zhou, *Nat. Commun.* **10**, 1-8 (2019).
11. J. Galego, C. Climent, F. J. Garcia-Vidal, J. Feist, *Phys. Rev. X* **9**, 021057 (2019).
12. T. E. Li, A. Nitzan, J. E. Subotnik, *J. Chem. Phys.* **152**, 234107 (2020).
13. I. Vurgaftman, B. S. Simpkins, A. D. Dunkelberger, J. C. Owrutsky, *J. Phys. Chem. Lett.* **11**, 3557-3562 (2020).
14. V. P. Zhdanov, *Chem. Phys.* **535**, 110767 (2020).
15. M. Du, J. A. Campos-Gonzalez-Angulo, J. Yuen-Zhou, *J. Chem. Phys.* **154**, 084108 (2021).
16. M. V. Imperatore, J. B. Asbury, N. C. Giebink, *J. Chem. Phys.* **154**, 191103 (2021).
17. X. Li, A. Mandal, P. Huo, *Nat. Commun.* **12**, 1315 (2021).
18. J. A. Campos-Gonzalez-Angulo, J. Yuen-Zhou, *J. Chem. Phys.* **156**, 194308 (2022).
19. J. A. Campos-Gonzalez-Angulo, J. Yuen-Zhou, *J. Chem. Phys.* **152**, 161101 (2020).
20. T. E. Li, A. Nitzan, J. E. Subotnik, *J. Chem. Phys.* **154**, 094124 (2021).
21. G. D. Wiesehan, W. Xiong, *J. Chem. Phys.* **155**, 241103 (2021).
22. R. S. Berry, *J. Chem. Phys.* **32**, 933-938 (1960).
23. J. F. Cahoon, K. R. Sawyer, J. P. Schlegel, C. B. Harris, *Science* **319**, 1820-1823 (2008).
24. F. H. Westheimer, *Acc. Chem. Res.* **1**, 70-78 (1968).
25. P. Törmä, W. L. Barnes, *Rep. Prog. Phys.* **78**, 013901 (2014).
26. B. Xiang *et al.*, *Proc. Natl. Acad. Sci. U.S.A.* **115**, 4845-4850 (2018).
27. B. Xiang *et al.*, *Science* **368**, 665-667 (2020).
28. B. Xiang, J. Wang, Z. Yang, W. Xiong, *Sci. Adv.* **7**, eabf6397 (2021).
29. B. Xiang, W. Xiong, *J. Chem. Phys.* **155**, 050901 (2021).
30. B. Xiang *et al.*, *J. Phys. Chem. A* **123**, 5918-5927 (2019).
31. D. Wellnitz, G. Pupillo, J. Schachenmayer, *Commun. Phys.* **5**, 1-11 (2022).
32. R. M. Hochstrasser, *Chem. Phys.* **266**, 273-284 (2001).
33. A. Tokmakoff *et al.*, *J. Chem. Phys.* **102**, 3919-3931 (1995).
34. P. Hamm, M. Zanni, *Concepts and methods of 2D infrared spectroscopy*. (Cambridge University Press, 2011).

35. A. D. Dunkelberger, B. S. Simpkins, I. Vurgaftman, J. C. Owrutsky, *Annu. Rev. Phys. Chem.* **73**, 429-451 (2022).
36. T. Botzung *et al.*, *Phys. Rev. B* **102**, 144202 (2020).
37. G. D. Scholes, *Proc. R. Soc. A* **476**, 20200278 (2020).
38. M. Du, J. Yuen-Zhou, *Phys. Rev. Lett.* **128**, 096001 (2022).
39. M. Khalil, N. Demirdöven, A. Tokmakoff, *J. Phys. Chem. A* **107**, 5258-5279 (2003).
40. D. V. Kurochkin, S. R. G. Naraharisetty, I. V. Rubtsov, *Proc. Natl. Acad. Sci. U.S.A.* **104**, 14209-14214 (2007).
41. P. Saurabh, S. Mukamel, *J. Chem. Phys.* **144**, 124115 (2016).
42. Z. Yang, B. Xiang, W. Xiong, *ACS Photonics* **7**, 919-924 (2020).
43. C. A. DelPo *et al.*, *J. Phys. Chem. Lett.* **11**, 2667-2674 (2020).
44. G. Khitrova, H. M. Gibbs, F. Jahnke, M. Kira, S. W. Koch, *Rev. Mod. Phys.* **71**, 1591 (1999).
45. J. A. Campos-Gonzalez-Angulo, R. F. Ribeiro, J. Yuen-Zhou, *New. J. Phys.* **23**, 063081 (2021).
46. A. D. Dunkelberger, R. B. Davidson, W. Ahn, B. S. Simpkins, J. C. Owrutsky, *J. Phys. Chem. A* **122**, 965-971 (2018).
47. B. Xiang *et al.*, *Sci. Adv.* **5**, eaax5196 (2019).
48. R. Houdré, R. P. Stanley, M. Ilegems, *Phys. Rev. A* **53**, 2711 (1996).
49. R. Duan, J. N. Mastron, Y. Song, K. J. Kubarych, *J. Phys. Chem. Lett.* **12**, 11406-11414 (2021).
50. R. F. Ribeiro *et al.*, *J. Phys. Chem. Lett.* **9**, 3766-3771 (2018).

**Acknowledgments:** The authors thank Harsh H. Bhakta for assisting with the Mathematica code.

**Funding:** T.-T.C. is supported by National Science Foundation DMR-1848215. Z.Y. is supported by AFSOR FA9550-21-1-0369. W.X. thanks the general support from Alfred P. Sloan Foundation FG-2020-12845. Acknowledgement is made to the donors of The American Chemical Society Petroleum Research Fund for M.D.'s support of this research through the ACS PRF 60968-ND6 Grant. J.Y.-Z. was supported by the US Department of Energy, Office of Science, Basic Energy Sciences, CPIMS Program under Early Career Research Program Award DE-SC0019188.

**Author contributions:** W. X. conceived the original idea and supervised the overall research. T.-T.C., Z.Y. and W.X. designed the experiments. T.-T.C. and Z.Y. conducted the experimental work. T.-T.C., M.D., J.Y.-Z. and W.X. analyzed data. M.D. and W.X. developed the anisotropy model. M.D. and J.Y.-Z. proposed mechanisms and developed spectral theory in SI section 4. T.-T.C. M.D., J.Y.-Z. and W.X. interpreted the results and wrote the manuscript.

**Competing interests:** Authors declare that they have no competing interests.

**Data and materials availability:** All data are available in the main text or the supplementary materials.